Effect of rotation on the equilibrium shapes and stability of liquid bridges in a lateral gravitational field

A. Laverón-Simavilla[1], V. Lapuerta[1], J. Rodríguez[1] and J. M. Perales[1]
[1] E.T.S.I.Aeronáuticos (Universidad Politécnica de Madrid), Spain, ana.laveron@upm.es, mariavictoria.lapuerta@upm.es

Abstract

A cylindrical liquid bridge supported between two circular-shaped disks in isorotation is considered. The effect of a lateral gravitational field on the stability of the liquid bridge is investigated. A numerical method is used to find stable and unstable shapes and to determine the stability limit for different values of lateral gravity.

1. Introduction

The behavior of liquid bridges has been widely studied, both theoretically and experimentally, due to the use of this configuration in a crystal growth technique known as the floating zone technique. In this technique, rotation of the supports is used to achieve an uniform temperature field.

In this paper a cylindrical liquid bridge supported between two circular-shaped disks in isorotation is considered. The effect of a lateral gravitational field on the stability of the liquid bridge is studied. Numerical and analytical studies for the case with rotation and no lateral gravity[1), 2)] have been made.

The stability limits and the equilibrium shapes of the configuration are calculated using an extension of an already implemented numerical method[3), 4)]. The numerical method is used to find stable and unstable shapes and to determine the stability limits for different values of the lateral gravity.

2. Problem description

The fluid configuration consists of a liquid bridge as sketched in Figure 1. The liquid column is held by surface tension forces between two disks of radius R_0, placed a distance L apart. Both disks are parallel and coaxial. The volume of the bridge is that corresponding to a cylindrical one, $V = \pi R_0^2 L$. The liquid bridge is in an lateral gravitational field, and is rotating at an angular speed Ω around the axis of the disks.

The equation governing the steady shape of the liquid bridge is obtained by balancing the different forces at the interface

$$\sigma\tilde{M}(R) + \tilde{P} + \frac{1}{2}\rho\Omega^2 R^2 + \rho|\boldsymbol{g}_l| R\cos\theta = 0 \qquad (1)$$

where $R = R(Z,\theta)$ is the equation of the gas-liquid interface, σ is the surface tension, $\tilde{M}(R)$ is twice the mean curvature of the interface, $\tilde{P}$ is the pressure difference at the origin, θ is the azimuthal angle, ρ is the liquid density, and $\boldsymbol{g}_l$ is the lateral gravity.

Equation (1) has to be integrated with the boundary conditions

$$R(\pm L/2, \theta) = R_0 \qquad (2)$$

$$R(Z,\theta) = R(Z,\theta + 2\pi) \qquad (3)$$

$$\frac{1}{2}\int_{-L/2}^{L/2} dZ \int_0^{2\pi} R^2(Z,\theta)\,d\theta = \pi L R_0^2 \qquad (4)$$

Eq. (2) indicates that the liquid column remains anchored to the disk edges, Eq. (3) comes from the azimuthal periodicity, and Eq. (4) expresses the conservation of the volume of the liquid bridge.

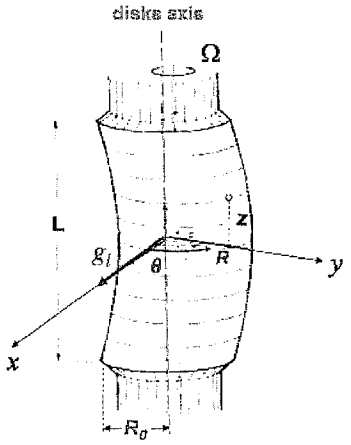

Figure 1. Geometry and coordinate system for the liquid bridge problem.

Let us introduce the following dimensionless variables and parameters

$$\Lambda = L/(2R_0),\ W = \rho\Omega^2 R_0^3/\sigma,$$
$$P = \tilde{P}R_0/\sigma,\ F(z,\theta) = R(z,\theta)/R_0, \qquad (5)$$
$$B_l = \rho|\boldsymbol{g}_l| R_0^{\,2}/\sigma,\ z = Z/R_0,$$

where Λ is the liquid bridge slenderness, W the Weber number, P the dimensionless reference pressure, and B_l is the lateral Bond number. The formulation of the problem then becomes:

$$M(F) + P + \frac{1}{2}WF^2 + B_l F\cos\theta = 0 \qquad (6)$$

with

$$M(F)=\frac{F(1+F_z^2)(F_{\omega\omega}-F)+FF_{zz}(F^2+F_\theta^2)-2F_\theta(F_\theta+FF_zF_{\omega\theta})}{\left(F^2(1+F_z^2)+F_\theta^2\right)^{3/2}} \tag{7}$$

The dimensionless boundary conditions for Eq. (6) are:

$$F(\pm\Lambda,\theta)=1 \tag{8}$$

$$F(z,\theta)=F(z,\theta+2\pi) \tag{9}$$

and

$$\int_{-\Lambda}^{\Lambda} dz \int_0^{2\pi} F^2(z,\theta)d\theta = 4\pi\Lambda \tag{10}$$

3. Numerical method

An algorithm, based on a continuation method[5] capable of stepping over bifurcation points and turning points was developed using a finite-difference method[3] and used to obtain the bifurcation diagrams and equilibrium shapes of liquid bridges subjected to lateral acceleration and other effects. The stable or unstable character of each of the shapes is determined to locate the stability limit. In this paper the system of equations (6)-(10) is solved by using an extension of that algorithm adapted to liquid bridges rotating around an eccentric axis to study the effect of combined eccentricity and angular rotation.

The method is based on linearizing Eqs. (7)-(11) around a known solution $(F_0(z,\theta),P_0)$ by seeking solutions of the form

$$F(z,\theta)=F_0(z,\theta)+f(z,\theta)+o(|f|),$$

$$P=P_0+p+o(|p|),$$

where $|f/F_0|<<1$ and $|p/P_0|<<1$. The leading order terms obtained from Eq. (7) result in an equation for $f(z,\theta)$

$$\tilde{O}^{-3/2}\left\{\tilde{A}+\left(\tilde{B}-\frac{3\tilde{A}\tilde{Q}}{2\tilde{O}}\right)f+\left(\tilde{C}-\frac{3\tilde{A}\tilde{S}}{2\tilde{O}}\right)f_z+\left(\tilde{D}-\frac{3\tilde{A}\tilde{T}}{2\tilde{O}}\right)f_\theta\right\}+ \tag{11}$$

$$+\tilde{E}f_{zz}+\tilde{G}f_{\theta\theta}+\tilde{H}f_{z\theta}+P_0+p+\frac{1}{2}W\left(F_0^2+2F_0f\right)+$$

$$+B_l(F_0+f)\cos\theta=0$$

where

$\tilde{A}$, $\tilde{B}$, $\tilde{C}$, $\tilde{D}$, $\tilde{E}$, $\tilde{G}$, $\tilde{H}$, $\tilde{O}$, $\tilde{Q}$, $\tilde{S}$ and $\tilde{T}$ are known functions of $F_0(z,\theta)$ and P_0 and thus of the particular point on the interface. The leading order terms obtained for the boundary conditions are

$$f(\pm\Lambda,\theta)=0 \tag{12}$$

$$f(z,\theta)=f(z,\theta+2\pi) \tag{13}$$

$$\int_{-\Lambda}^{\Lambda} dz \int_0^{2\pi} F_0(z,\theta)^2 d\theta + 2\int_{-\Lambda}^{\Lambda} dz \int_0^{2\pi} [F_0(z,\theta)f(z,\theta)]d\theta = 4\pi\Lambda \tag{14}$$

If $(F_0(z,\theta),P_0)$ is an exact solution of the problem, Eqs. (11)-(14) can be simplified, but all terms have been retained here because $(F_0(z,\theta),P_0)$ will only be an approximation to the solution in the iterative scheme used here.

In order to develop a center finite difference scheme the domain has been characterized by a mesh, defined as the intersection of the free surface with the following planes:

$$z=\Lambda\left(\frac{2j}{J}-1\right),\quad j=0,1,...,J\ , \tag{15}$$

$$\theta=\frac{2\pi}{I+1}i,\quad i=0,1,...,I\ , \tag{16}$$

By doing so, the system (11)-(14) yields a linearized system of finite-difference equations which can be written as follows:

$$\alpha_{ij}f_j^i+\beta_{ij}f_{j-1}^i+\gamma_{ij}f_{j+1}^i+\delta_{ij}f_j^{i-1}+\varphi_{ij}f_j^{i+1}$$

$$+\phi_{ij}(f_{j+1}^{i+1}-f_{j+1}^{i-1}-f_{j-1}^{i+1}+f_{j-1}^{i-1})+p=\psi_{ij},\quad i=0,...,I,\quad j=0,...,J \tag{17}$$

$$f_j^0-f_j^{I+1}=0 \tag{18}$$

$$f_J^i=1-F_{0,J}^i,\qquad i=0,...,I \tag{19}$$

$$f_0^i=1-F_{0,0}^i,\qquad i=0,...,I \tag{20}$$

$$\sum_{i=0}^{I}\sum_{j=0}^{J}a_{ij}f_j^i=A \tag{21}$$

where the coefficients α_{ij}, β_{ij}, γ_{ij}, δ_{ij}, φ_{ij}, ϕ_{ij}, ψ_{ij}, a_{ij} and A are functions of $F_{0,j}^i$ and P_0.

The iterative scheme is started from a known solution $(F_o,P_o,\Lambda,W=0,B_l=0)$, which is introduced into equations (17)-(21). The value of the Weber number is then increased by a small amount $(W=W_1)$, and the linear terms (f,p) are calculated. The new values

$$(F_o=F_o+f,P_o=P_o+p,\Lambda,W=W_1,B_l=0)$$

are then introduced into equations (17)-(21) to obtain new corrections (f,p), and this procedure is repeated until $\|f\|^2+p^2\le 10^{-6}$ and the final equilibrium shape is obtained

$(F_1=F_o+f,\ P_1=P_o+p,\quad \Lambda,\ W=W_1,B_l=0)$.

The iteration then repeats with an increased value of the Weber number $(W=W_2)$ giving a new equilibrium shape

$$(F_2=F_o+f,P_2=P_o+p,\Lambda,W=W_2,B_l=0).$$

All equilibrium shapes obtained in this manner are stored to be used as initial conditions for an iterative scheme identical to the one just described, but with increasing values of the eccentricity, e. Together, these procedures allow the bifurcation diagram to be completed.

If no further modifications are made, the algorithm becomes unstable when crossing a critical point. To stabilize the algorithm a supplementary

equation defining the arc-length parameter needs to be included. The details of the numerical method used to locate bifurcation and limit points are identical to those outlined elsewhere[3] and will not be repeated here. We only remark that an analysis of the errors of the numerical method was made[3], which indicates that a minimum number of mesh points is needed to find the complete bifurcation diagram and that this minimum increases as the slenderness of the liquid bridge decreases. The size of the mesh used to obtain the results presented in this paper is IxJ=19x28.

4. Results

Perales et al. [1] looked for a solution of Eqs. (1)-(4) with B_l=0 of the form: F=1+εf +o(ε), P=1-W/2+εp +o(ε), ε<<1 (small departures from a cylindrical liquid bridge), finding the non-zero solutions:

(i) Non-axisymmetric shapes (C-mode)

$$W_0=\left(\frac{\pi}{2\Lambda}\right)^2,\quad f=\cos\theta\cos\left(\frac{\pi}{2\Lambda}z\right),\quad p=0$$

(ii) Axisymmetric shapes (amphora mode)

$$W_0=\left(\frac{\pi}{\Lambda}\right)^2-1,\quad f=\sin\left(\frac{\pi}{\Lambda}z\right),\quad p=0$$

The functions $W_0(\Lambda)$ represent in the Λ-W plane the curves where the transition between stable and unstable equilibrium shapes appears. These two curves have been plotted in Figure 2. The point B, for which expressions (24) and (25) are equal ($\Lambda=\sqrt{3}\pi/2$), marks the transition between the C-mode and the amphora mode instabilities.

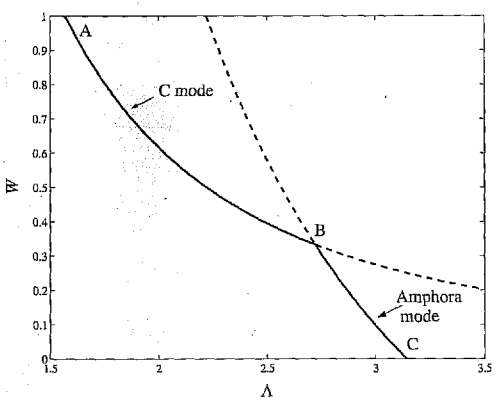

Figure 2. Stability diagram for zero lateral gravity.

The bifurcation diagrams are sketched in Figure 3 and Figure 4 for B_l=0. Note that the bifurcations are both subcritical and hence that both equilibrium shapes (the C-mode shape and the amphora mode shape) are unstable.

If the rotation speed is slowly increased from zero, one has stable cylindrical shapes until W reaches W_0 at which point an instability occurs. Thus, for B_l=0 liquid bridges with $\Lambda<\sqrt{3}\pi/2$ lose stability to a non-axisymmetric mode and liquid bridges with $\Lambda>\sqrt{3}\pi/2$ lose stability to an axisymmetric mode.

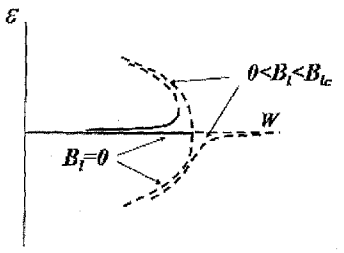

Figure 3. Bifurcation diagram for $\Lambda<\sqrt{3}\pi/2$.

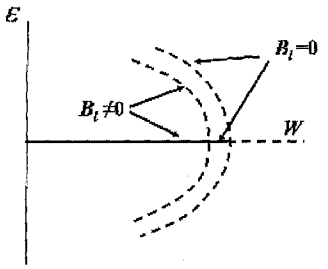

Figure 4. Bifurcation diagram for $\Lambda>\sqrt{3}\pi/2$.

With the numerical method we have recovered the stability threshold for $B_l=0$, and we have analyzed the dependency of this threshold on the lateral gravity and the angular speed. Figure 5 shows the variation of the stability threshold for increasing lateral gravity. The line for $B_l=0$ corresponds to the threshold represented in Figure 2. As we can see in the figure, for small values of the lateral gravity, it has a somewhat stronger effect on short liquid bridges ($\Lambda<\sqrt{3}\pi/2$), although for increasing values of the lateral gravity the stability region is strongly reduced even for long liquid bridges ($\Lambda>\sqrt{3}\pi/2$).

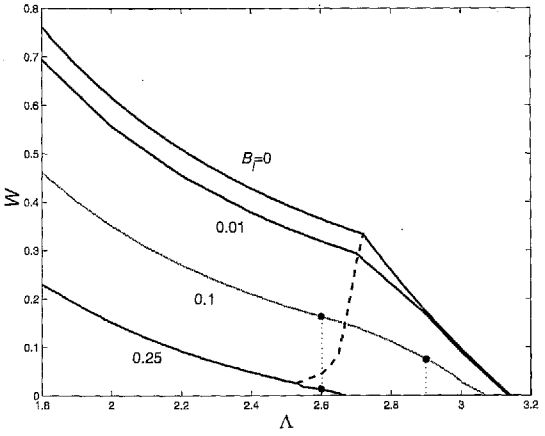

Figure 5. Stability threshold for different values of B_l. The dashed line marks the transition between a subcritical pitchfork bifurcation (B) and a turning point (TP).

The analysis shows a complex behaviour of the instability boundary for liquid bridges. For a given liquid bridge with $\Lambda<\sqrt{3}\pi/2$, increasing the

lateral gravity leads to:

(i) A subcritical pitchfork bifurcation (for B_l=0).

(ii) A turning point (for $0<B_l<B_{lc}$). The bifurcation diagram has been sketched in Figure 3.

(iii) A subcritical pitchfork bifurcation (for $B_{lc} < B_l$).

The region in the angular rotation corresponding to the turning point instability decreases as Λ increases, disappearing for $\Lambda = \sqrt{3}\pi/2$, the point where the transition between C-mode and amphora mode occurs for B_l=0.

For $\Lambda > \sqrt{3}\pi/2$ the effect of lateral gravity does not change the character of the initial instability, as happened for the C-mode. Instead, a subcritical pitchfork bifurcation persists, as in the B_l =0 case. The bifurcation diagram has been sketched in Figure 4.

Fig. 5 shows the variation of the stability threshold for increasing lateral gravity. The dashed line marks the change of the primary instability from subcritical pitchfork bifurcation (region B in the figure) to turning point (region TP in the figure).

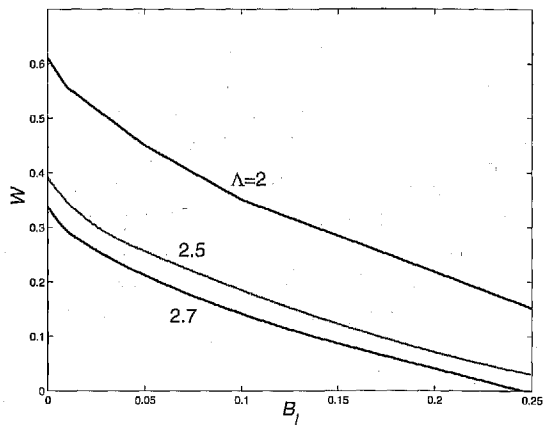

Figure 6. Effect of the lateral gravity and the slenderness on the stability threshold.

Figure 7 and Figure 8 show the bifurcation diagrams obtained by representing the area of the section at z=0 and z=Λ/2 respectively, as a function of W for Λ=2.6 and two values of lateral gravity marked in Figure 5: B_l=0.1, which corresponds to the turning point and B_l=0.25, which corresponds to the subcritical pitchfork bifurcation. The stable part of the branches is represented with a solid line, and the unstable part with a dashed line.

Figure 9 and Figure 10 show the equilibrium shapes for the cases indicated in Figure 7 and Figure 8, respectively. In Figure 10, equilibrium shapes for both the main branch and the bifurcated one are represented. As we can see in both figures, the stable shapes are non-axisymmetric modes (that is, C-modes). The behaviour of the equilibrium shapes for the two possibilities with $\Lambda < \sqrt{3}\pi/2$ is as follows:

(i) For both the pitchfork bifurcation point with B_l=0 and the turning point with $0<B_l<B_{lc}$ the associated eigenfunction is non-axisymmetric (that is, a C-mode) so that the breaking process can be expected to lead to a non-axisymmetric configuration.

(ii) For the subcritical pitchfork bifurcation point with $B_{lc}< B_l$ the associated eigenfunction is axisymmetric (that is, an amphora-mode) so that the breaking process can be expected to lead to a combined amphora and C-mode configuration.

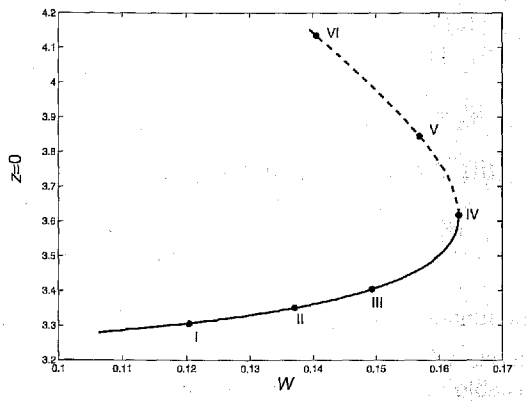

Figure 7. Bifurcation diagram for $\Lambda = 2.6$ and $B_l = 0.1$.

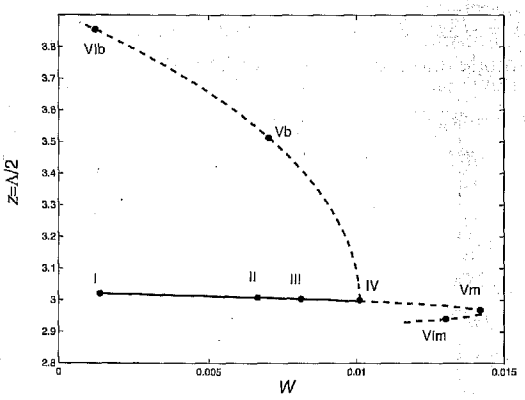

Figure 8. Bifurcation diagram for $\Lambda = 2.6$ and $B_l = 0.25$.

Figure 11 shows the bifurcation diagram obtained by representing the area of the section at z=-Λ/2 as a function of W for Λ=2.9 and B_l=0.1 (marked in Figure 5), which corresponds to the subcritical pitchfork bifurcation. The stable part of the branches is represented with a solid line, and the unstable part with a dashed line.

Figure 12 shows the equilibrium shapes for the cases indicated in Figure 11.

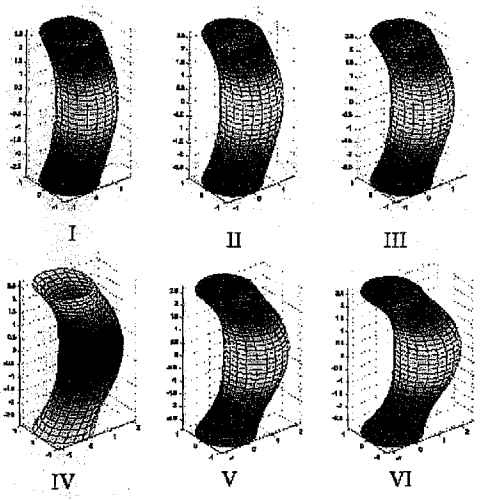

Figure 9. Evolution of the equilibrium shapes for $\Lambda = 2.6$ along the main solution branch for $B_l = 0.1$. Shapes I to IV are stable while V and VI are unstable.

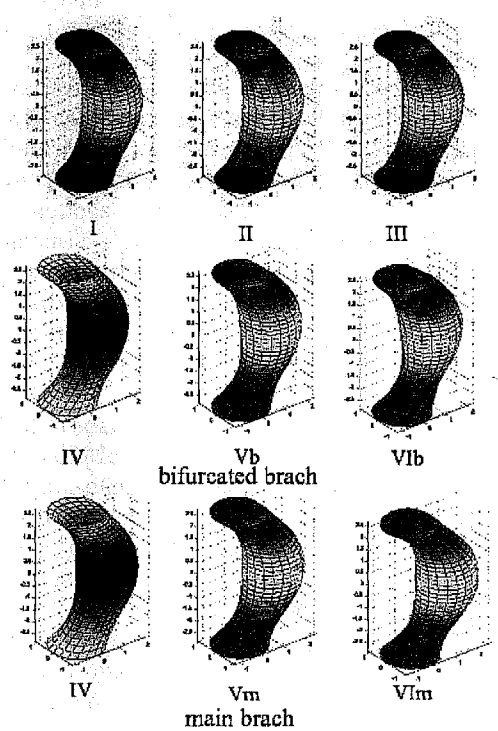

Figure 10. Evolution of the equilibrium shapes of a cylindrical liquid bridge with Λ=2.6 along the main branch and the bifurcated one for $B_l = 0.25$. Shapes I to IV are stable and the rest are unstable.

The results obtained here for liquid bridges in isorotation in a lateral gravity field can be compared with those obtained for liquid bridges rotating around an eccentric axis[6), 7)], as both effects correspond to lateral forces. The comparison shows that, although the stability behaviour is similar, lateral gravity has a stronger effect for long liquid bridges ($\Lambda < \sqrt{3}\pi/2$). For example, liquid bridges in isorotation with $\Lambda > 2.7$ cannot support lateral gravity with $B_l > 0.25$, that is, they are unstable for any value of $B_l > 0.25$, while for non-lateral gravity the same liquid bridges can support eccentric rotation for any value of the eccentricity, although the limit value of the rotation rate decreases as the distance between the axis of the disk and the axis of rotation increases. The explanation for this is that the lateral force induced by eccentric rotation is proportional to the rotation rate, while the force of the lateral gravitational field is independent of the rotation rate.

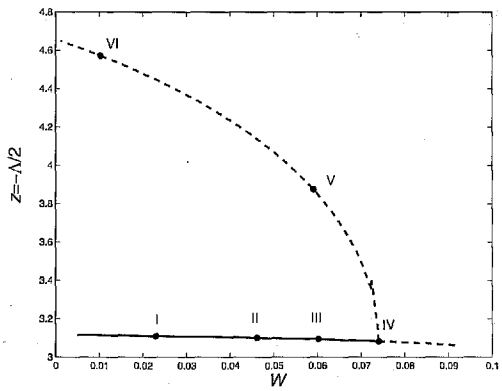

Figure 11. Bifurcation diagram for $\Lambda = 2.9$ and $B_l = 0.1$.

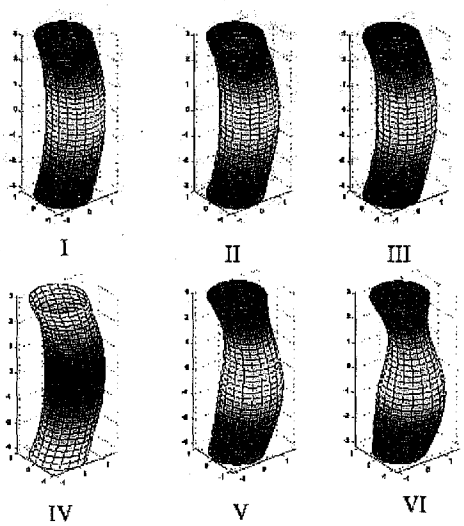

Figure 12. Evolution of the equilibrium shapes of a cylindrical liquid bridge with Λ=2.9 along the bifurcated branch for $B_l = 0.1$. Shapes I to IV are stable and the rest are unstable

5. Conclusions

The stability limits of liquid bridges in a lateral gravitational field rotating around an eccentric axis have been calculated numerically. The numerical method is used to find stable and unstable shapes and to determine the dependence of the stability threshold on the slenderness and the strength of the lateral gravity.

The effect of lateral gravity is to drastically reduce the stability region. Gravity affects short liquid bridges more, although for increasing values of the gravitational field the stability region is also strongly reduced for long liquid bridges.

Acknowledments

This work has been sponsored by the Ministerio de Educación y Ciencia (MEC) and is part of a more general endeavor for the study of fluid physics in processing under microgravity (Proyect No. MEC ESP2007-65221). The authors want to thank Jeff Porter for his help.

References

1) Perales, J. M., Sanz, A. and Rivas D., *Appl. Microgravity Tech. II,* **4**, 193, 1990.
2) Vega, J. M. and Perales, J. M., *ESA SP-191*, ESA, Paris, 247, 1983.
3) Laverón-Simavilla; A., Perales, J. M. , *Phys. Fluids*, **7**, 1204, 1995.
4) Laverón-Simavilla; A., Checa, E., *Phys. Fluids*, **9**, 817, 1997.
5) Keller, H. B., "Lectures on Numerical Methods in Bifurcation Problems", Springer-Verlag, Berlin, 1987.
6) Laverón-Simavilla, A., Lapuerta, V., Rodríguez, J. and González, M. A., *Fluid Dynamics and Materials Processing*, **III**, 1, 2008.
7) Lapuerta, V., Laverón-Simavilla, A., Rodríguez, J. and González, M. A., *Advance in Space Research*, (in press).